Science of the Total Environment 806 (2022) 151414

Contents lists available at ScienceDirect

Science of the Total Environment

journal homepage: www.elsevier.com/locate/scitotenv

Integral analysis of hydrodynamic cavitation effects on waste activated sludge characteristics, potentially toxic metals, microorganisms and identification of microplastics

Sabina Kolbl Repinc [a], Benjamin Bizjan [b], Vaibhav Budhiraja [c], Matevž Dular [b], Jurij Gostiša [b], Barbara Brajer Humar [d], Anela Kaurin [e], Andrej Kržan [c], Marjetka Levstek [d], Juan Francisco Morales Arteaga [e], Martin Petkovšek [b], Gašper Rak [a], Blaž Stres [a,f,g], Brane Širok [b], Ema Žagar [c], Mojca Zupanc [b,*]

[a] Faculty of Civil and Geodetic Engineering, University of Ljubljana, Ljubljana, Slovenia
[b] Faculty of Mechanical Engineering, University of Ljubljana, Ljubljana, Slovenia
[c] Department of Polymer Chemistry and Technology, National Institute of Chemistry, Ljubljana, Slovenia
[d] JP CCN Domzale-Kamnik d.o.o., Domzale-Kamnik WWTP, Domzale, Slovenia
[e] Biotechnical Faculty, Agronomy Department, University of Ljubljana, Ljubljana, Slovenia
[f] Biotechnical Faculty, Department of Animal Science, University of Ljubljana, Ljubljana, Slovenia
[g] Jozef Stefan Institute, Department of Automation, Biocybernetics and Robotics, Ljubljana, Slovenia

HIGHLIGHTS

- Efficient disintegration and solubilization of WAS with novel PD RGHC were reached.
- Microjets and shear forces caused mechanically cracked, torn off and split cells.
- Increased soluble COD, NH_4-N and NO_3-N confirmed release of intracellular DOM.
- PTM concentrations (most dominant for Pb) were affected by chemical effects of HC.
- PE, PP, PET, and PA-6 microplastics were identified in the sludge sample.

GRAPHICAL ABSTRACT

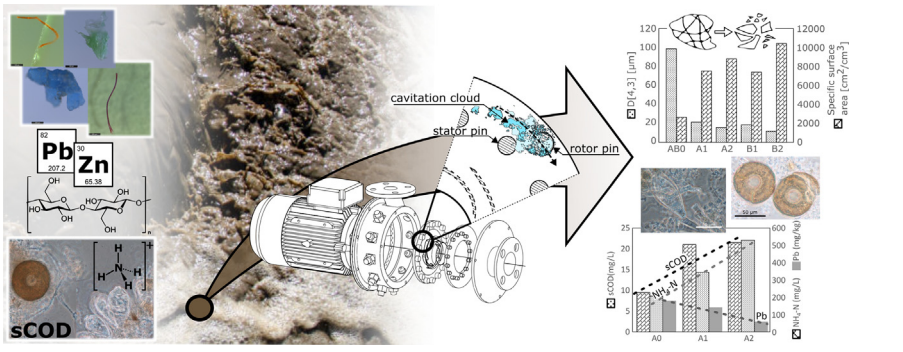

ARTICLE INFO

Article history:
Received 29 September 2021
Received in revised form 26 October 2021
Accepted 30 October 2021
Available online 4 November 2021

Editor: Huu Hao Ngo

ABSTRACT

Wastewater treatment plants, the last barrier between ever-increasing human activities and the environment, produce huge amounts, of unwanted semi-solid by-product - waste activated sludge. Anaerobic digestion can be used to reduce the amount of sludge. However, the process needs extensive modernisation and refinement to realize its full potential. This can be achieved by using efficient pre-treatment processes that result in high sludge disintegration and solubilization. To this end, we investigated the efficiency of a novel pinned disc rotational generator of hydrodynamic cavitation. The results of physical and chemical evaluation showed a reduction in mean particle size up to 88%, an increase in specific surface area up to 300% and an increase in soluble COD,

Abbreviations: COD, total chemical oxygen demand; DD, disintegration degree; DO, dissolved oxygen; DOM, dissolved organic matter; cDOM, chromogenic dissolved organic matter; DR, disintegration rate; EPS, extracellular polymeric substances; Ex-Em, excitation-emission; HC, hydrodynamic cavitation; MP, microplastics; MW, molecular weight; N_p, number of cavitation passes; PA-6, polyamide - 6; PD, pinned discs; PE, polyethylene; PET, polyethylene terephthalate; PP, polypropylene; PTM, potentially toxic metals; ROS, reactive oxygen species; RGHC, rotational generator of hydrodynamic cavitation; sCOD, soluble chemical oxygen demand; SDS, sodium dodecyl sulfate; SE, specific energy; SESS, specific energy of sludge solubilization; sTOC, soluble total organic carbon; TS, total solids; TW, tap water; WAS, waste activated sludge; WW, wastewater; WWTP, wastewater treatment plant.

* Corresponding author.
E-mail address: mojca.zupanc@fs.uni-lj.si (M. Zupanc).

https://doi.org/10.1016/j.scitotenv.2021.151414

Keywords:
Hydrodynamic cavitation
Waste activated sludge
Sludge characteristics
Microbial damage
Potentially toxic metals
Microplastics

NH_4-N, NO_3-N, PO_4-P up to 155.8, 126.3, 250 and 29.7%, respectively. Microscopic images confirmed flocs disruption and damage to yeast cells and *Epistilys species* due to mechanical effects of cavitation such as microjets and shear forces. The observed cell ruptures and cracks were sufficient for the release of small soluble biologically relevant dissolved organic molecules into the bulk liquid, but not for the release of microbial DNA. Cavitation treatment also decreased total Pb concentrations by 70%, which was attributed to the reactions triggered by the chemical effects of cavitation. Additionally, the study confirmed the presence of microplastic particles and fibers of polyethylene, polyethylene terephthalate, polypropylene, and nylon 6 in the waste activated sludge.

1. Introduction

Before it is released into the environment, municipal wastewater (WW) is treated in wastewater treatment plants (WWTP), usually using the biological activated sludge process. Unfortunately, the end product of this process are large quantities of excess waste activated sludge (WAS), reaching several million tonnes per year in the EU alone (Iyare et al., 2020; Khanh Nguyen et al., 2021). The efficient management of these large volumes of WAS represents one of the major operational costs for urban WWTPs today (Khanh Nguyen et al., 2021; Kim et al., 2020).

WAS application to agricultural land and anaerobic digestion are two of the most used options for sludge disposal (Khanh Nguyen et al., 2021). For example, application of WAS to cropland has been shown to improve crop productivity by increasing soil organic matter and nutrient content, increasing microbial biomass, and improving soil physical properties (Geng et al., 2020). However, due to the retention of toxic organic chemicals, pathogens, potentially toxic metals (PTMs) and microplastics (MP), the reuse of untreated WAS for agricultural purposes is no longer recommended (Iyare et al., 2020; Khanh Nguyen et al., 2021; Collivignarelli et al., 2019). PTMs can be toxic even at low concentrations, are difficult to remove and can easily accumulate in organisms. In the European Union, the use of WAS in agriculture is regulated by the permissible limits of PTMs. According to EU Directive 86/278/EEC (86/278/EEC) and Slovenian legislation (Official Gazette of the Republic of Slovenia: 62/2008), municipal wastewater sludge cannot be used on agricultural land if the concentration exceeds the limits of 1.5, 200, 300, 1.5, 75, 250 and 1200 mg/kg (dry weight) for Cd, total Cr, Cu, Hg, Ni, Pb and Zn, respectively. Some of the metals have carcinogenic, mutagenic and/or teratogenic potential in humans. Most toxic metals and metalloids are As, Cd, Cr, Cu, Hg, Mn, Ni, Pb and Zn (Ali et al., 2019; Sabouhi et al., 2020). Together with PTM, the presence of another emerging pollutant - microplastics (MP), the retention of which in WAS has been repeatedly reported (Iyare et al., 2020), additionally hinders the use of WAS in agriculture. According to Slovenian regulations, up to 2% and 0.5% (dry weight) of plastics larger than 2 mm are allowed in digestate and compost, respectively (Kisser et al., 2020). MP, classified as synthetic polymer particles ranging in size from a few μm to 5 mm (Iyare et al., 2020), includes two types: primary and secondary. Primary MP are particles intentionally produced for use, such as particles added to cosmetic products, while secondary MP result from fragmentation of larger plastic wastes, such as expanded polystyrene products, fibers shed from textiles, fishing gear, etc., and rubber particles derived from vehicle tire wear. WWTPs represent a critical step in the flow of WW containing microplastics and can be a major source of MP particles and microfibers, either via effluent or WAS (Iyare et al., 2020).

The second option available to WWTPs to deal with the excess WAS is anaerobic digestion (Khanh Nguyen et al., 2021). To improve anaerobic digestion and increase biogas production, various pre-treatment methods such as biological, mechanical, thermal, and chemical processes can be used (Khanh Nguyen et al., 2021; Carrère et al., 2010). They facilitate anaerobic digestion by breaking cell walls, releasing their internal contents, and improving WAS solubilization (Kim et al., 2020). Acoustic and hydrodynamic cavitation have been described as suitable mechanical pre-treatment methods (Khanh Nguyen et al., 2021; Carrère et al., 2010; Bhat and Gogate, 2021), and have been shown to increase biogas production in numerous studies (Bhat and Gogate, 2021; Petkovšek et al., 2015). Cavitation is a physical phenomenon in which small vapour bubbles are formed in a liquid due to a local pressure drop. When the bubbles formed collapse, large amounts of energy are released in a very small spatial and temporal region, triggering the mechanical (i.e., high temperatures, shear forces, microjets, and shock waves) and chemical (formation of predominantly •OH) effects associated with cavitation (Benito et al., 2005). The extreme conditions created by the collapse of cavitation bubble provide a unique environment that can be exploited in a variety of ways, from disintegration of WAS (Kim et al., 2020; Petkovšek et al., 2015) to the degradation of organic micropollutants (Zupanc et al., 2014) to the destruction of microorganisms and viruses (Zupanc et al., 2019).

Nowadays hydrodynamic cavitation (HC) is gaining attention as an effective, easily scalable, and cost-effective process (Bhat and Gogate, 2021). There are many different HC designs used for WW and WAS treatment, such as orifice plates, venturi tubes, and rotational generators of hydrodynamic cavitation (RGHCs) (Bhat and Gogate, 2021; Wang et al., 2021). Compared to venturi and orifice designs, RGHCs have lower specific energy consumption, allow for better scalability, do not require a separate high-pressure pump, and still achieve similar cavitation intensity (Wang et al., 2021). There are many different RGHC designs being investigated, such as dimpled rotors (Kim et al., 2020; Kim et al., 2019; Zubrowska-Sudol et al., 2020), serrated discs (Petkovšek et al., 2015; Vilarroig et al., 2020) and pinned discs (PD) (Gostiša et al., 2021a). Dimpled rotors and serrated discs have already shown positive effects on WAS disintegration, while the PD RGHC design has only recently been developed and its hydrodynamic properties published (Gostiša et al., 2021a). Compared to other designs, PD RGHC has the advantage of better scalability and higher cost efficiency of WW treatment in terms of cost per volume of treated WW and per unit mass of removed COD (Gostiša et al., 2021a; Gostiša et al., 2021b). Although the potential of cavitation as an efficient WAS pretreatment method has been repeatedly determined at lab-scale (Bhat and Gogate, 2021), to the authors knowledge there is only one study besides ours that evaluates HC for WAS disintegration at pilot-scale (Vilarroig et al., 2020). The lack of these studies is responsible for the gap that exists between lab-scale and industrial scale, which is why studies like ours are of utmost importance.

The aim of this study was to evaluate the potential of a novel pilot-scale PD RGHC as a mechanical pre-treatment method for efficient WAS disintegration. The effects of two RGHC regimes were assessed by performing 1.) physical evaluation (i.e. particle size and distribution analysis, microscopic analysis), 2.) chemical evaluation (i.e. WAS characteristics analysis, dissolved organic matter spectral analysis, microbial DNA analysis) and 3.) PTM evaluation (i.e. total metal concentration determination, evaluation of bioavailability by sequential extraction) of WAS samples before and after cavitation. Additionally, the determination and identification of MP particles and fibers in WAS samples was performed.

2. Materials and methods

2.1. Waste activated sludge (WAS)

The initial WAS was taken from a secondary sedimentation tank of an aerobic biological stage treating municipal and industrial WW at the Domžale - Kamnik WWTP. Thickened WAS with at least 1.5% total solids (TS) content was used for the experiments. The main WAS characteristics before the HC experiments are presented in Table 3 and the Supplementary material, Suppl. 1 (sample AB0: initial, non-cavitated WAS).

2.2. Hydrodynamic cavitation set-up

The effects of the PD RGHC on WAS were investigated on a set-up with a pinned disc rotating generator of hydrodynamic cavitation (PD RGHC) previously described by Gostiša and co-workers (Gostiša et al., 2021a), (Gostiša et al., 2021b) shown in Fig. 1. PD RGHC comprised integrated pump impeller and cavitation inducing elements (discs with multiple pin-shaped protrusions equidistantly distributed on the disc circumference, Fig. 2 – 1) to induce cavitation in the wake region behind the pins (Fig. 1 - right). For details on the RGHC design, please refer to the Supplementary material, Suppl. 2.

The PD RGHC was driven by a variable frequency drive-powered AC motor (Fig. 2 - 2) and was installed in a closed-loop pipeline with a 1000 L reservoir (Fig. 2 - 3). The liquid ambient pressure (p_0) near the cavitation zone was measured with the absolute pressure transducer (Fig. 2 – a), while the pressure head across the RGHC (Δp) was measured with the differential pressure transducer (Fig. 2 – b), both model ABB 2600 T. Flow rate was measured using an electromagnetic flowmeter ABB WaterMaster DN40 (Fig. 2 – c) and samples were collected through the outlet valve (Fig. 2 - 4).

Based on the evaluation of hydrodynamic and cavitation characteristics of the RGHC on TW and proved favourable conditions for COD removal from WW (Gostiša et al., 2021b), two different operating regimes and corresponding RGHC layouts (namely, layouts A and B) were chosen (Table 1). Both layouts were selected in the fully developed cavitating flow regime to achieve efficient WAS disintegration/solubilization and determine if the process is sensitive to modification of operating parameters such as rotor speed and pin diameter. Although the visualization in WW in that study was insufficient to draw firm conclusions, pressure pulsation measurements indicated that there was a difference between selected cavitating regimes (Fig. 3). A more detailed description of the visualization and pressure measurement analysis can be found in the study by Gostiša and co-workers (Gostiša et al., 2021b) and the results presented in Fig. 3 are a summary of the tests performed for the purpose of that study. All conditions were chosen near the motor's rated rotational speed of 3000 RPM and power 6.3–6.5 kW to maximize the cavitation intensity.

To compare the efficiency of the two selected PD RGHC regimes (Table 1), the initial WAS sample (AB0) was the same for both HC experiments (A and B). More detailed description of the experimental procedure is given in the Supplementary material, Suppl. 2.

Energy efficiency was estimated by introduction of two characteristic WAS solubilization parameters as suggested by Villaroig and co-workers (Vilarroig et al., 2020):

a) Specific energy (SE) per mass unit of TS treated

$$SE = \frac{P \cdot t}{V \cdot TS} \quad (1)$$

b) Specific energy of sludge solubilization (SESS)

$$SESS = \frac{P \cdot t}{V \cdot (sCOD_f - sCOD_i)} \quad (2)$$

In Eqs. (1) and (2), P (kW) is the electrical power required to operate RGHC, t (min) is the cavitation time, V (L) is the batch volume of cavitated sludge, TS (g/L) is the initial total solids concentration. $sCOD_f$ (mg/L) represents the soluble COD of the disintegrated final sample and $sCOD_i$ (mg/L) represents the soluble COD of the initial sample (AB0). The parameters SE and SESS are listed in Table 7 in comparison with studies by other authors.

2.3. Sample preparation and analyses

Physical and chemical evaluation analyses were performed to determine the effectiveness of the two HC regimes. For particle size and distribution and microscopic analysis 200 mL of the WAS sample was taken, 100 mL for each analysis. For determination of WAS characteristics, spectral and microbial DNA analysis 1.5 L WAS sample was taken. For PTM analysis, 20 L WAS samples were collected. For these analyses, samples were collected before HC experiments and after 15 and 30 Np, respectively. For the analysis of microplastics, 1 L samples were collected only before the HC experiments and after 30 Np. After 15 Np, approximately 22 L of sample was collected for the analyses described above, which was considered in the treatment time for the remaining 15 Np at a constant flow rate.

2.3.1. Physical evaluation

2.3.1.1. Particle size and distribution analysis. Particle size and distribution experiments of non-cavitated and cavitated WAS samples were performed with the Analysette 22 MicroTec Laser Particle sizer - Wet Dispersion Unit (Fritsch, Germany) according to the previously

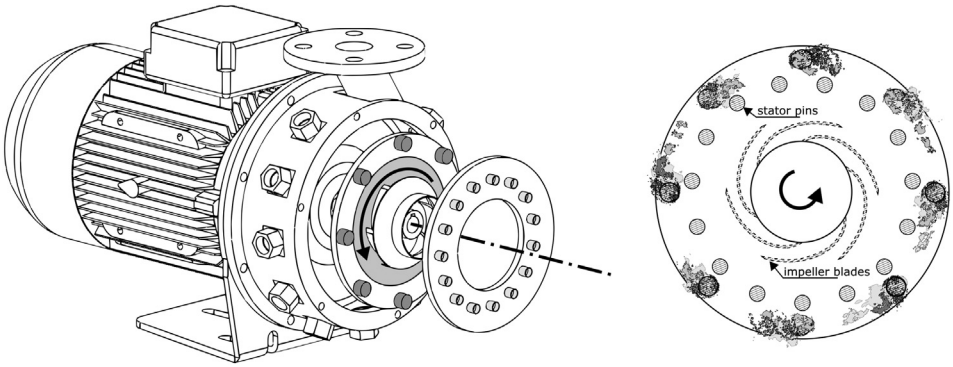

Fig. 1. Pinned disc RGHC design with visible cylindrical stator and rotor pins (left) and cavitation vortices in the low-pressure wake behind the pins (right).

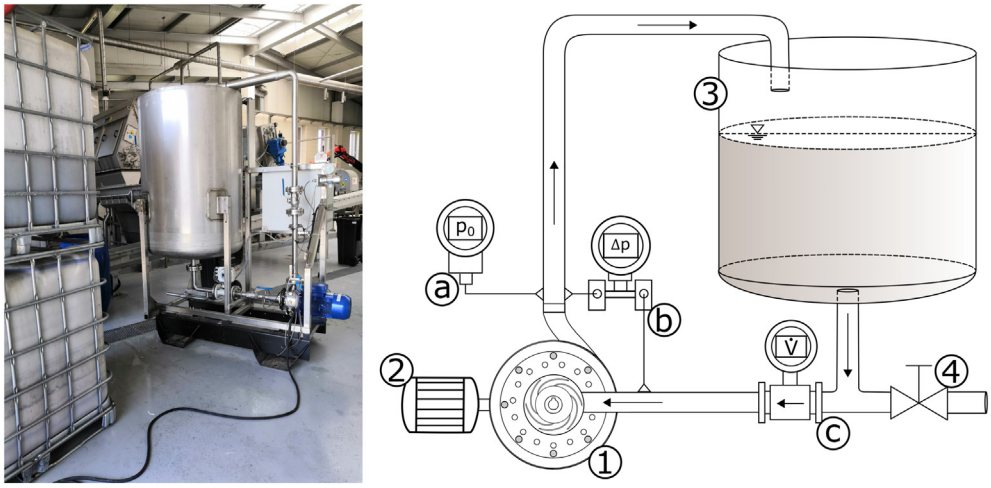

Fig. 2. Left: experimental set-up image (upper left container with AB0 WAS sample); Right: experimental RGHC set-up scheme: 1 – PD RGHC, 2 – electric motor controlled by a variable frequency drive, 3–1000 L reservoir, 4 – discharge valve, a – absolute pressure transducer, b – differential pressure transducer, c -electromagnetic flow meter.

described particle size analysis ISO 13320 - Laser Diffraction Methods (Kolbl et al., 2016). Percentile particle sizes of 10%, 50% and 90% were calculated and expressed as d10, d50 and d90, respectively. Mean particle size was expressed as D[4,3].

2.3.1.2. Microscopic analysis. Phase-contrast images of non-cavitated and cavitated WAS samples, flocs, and individual microorganisms, were taken using a microscope Nikon Eclipse 80i at magnifications of 100×, 200×, 400× and 1000×. A drop of the sample was placed on a microscopic glass slide, spread evenly on the surface, and observed under the microscope. If the particle concentration was high, the samples were additionally diluted with water.

2.3.2. Chemical evaluation

2.3.2.1. Analysis of WAS characteristics. Before and after HC treatments, measurements of pH, dissolved oxygen (DO), conductivity, salinity and temperature were performed at the site of experiments. The details of the equipment are given in Supplementary material, Suppl. 1.

For WAS characterization of the non-cavitated and cavitated samples, chemical analyses of the total and/or soluble fractions were performed in duplicates and are given as average values with standard deviations. For the soluble fraction, samples were centrifuged at 15,000 rpm for 20 min and the supernatant was used. In short, soluble COD (sCOD), TOC (sTOC), NO_3-N and NO_2-N were measured using LCK 114, 386, 340 and 341 cuvette tests (Hach-Lange, Germany), respectively. Soluble NH_4-N and PO_4-P were determined according to Method 8038 and 8178 (Hach-Lange, Germany), respectively. DR/2800 spectrophotometer (Hach-Lange, Germany) was used for analysis. Additional information is given in Supplementary material, Suppl. 1.

Disintegration degree (DD) also known as solubilization rate of WAS was calculated from the following equation (Khanal et al., 2007; Erden and Filibeli, 2010):

$$DD = \left(\frac{sCOD_f - sCOD_i}{sCOD_{max} - sCOD_i}\right) \cdot 100 \quad (3)$$

where $sCOD_f$ (mg/L) is the average value of soluble COD of the final disintegrated sample, $sCOD_i$ (mg/L) is the average value of soluble COD of the initial non-cavitated sample, and $sCOD_{max}$ (mg/L) is the average value of soluble COD after chemical disintegration with NaOH. For chemical disintegration, 1 M NaOH (Sigma-Aldrich, Germany) was added to the initial sample at a ratio of 1:2 and heated at 90 °C for 10 min. The value of $sCOD_{max}$ was 4480 ± 113 mg/L. The value of DD is given in Tables 3 and 7, while disintegration rate DR = DD/t (%/h) is given in Table 7.

Linear Pearson's correlation and statistical significance were calculated in software PAST (Φyvind et al., 2001) to see the correlations between Np and measured physical (particle size and distribution) and chemical (soluble COD, TOC, NH_4-N, NO_3-N, PO_4-P) parameters of non-cavitated and cavitated WAS samples.

2.3.2.2. UV-VIS and Ex-Em spectral analysis of biologically relevant dissolved organic matter (DOM). The molecular weight (MW) of dissolved organic matter (DOM) was characterized using spectrophotometric measurements according to Helms and co-workers (Helms et al., 2009) and Twardowski and co-workers (Twardowski et al., 2004). In short, non-cavitated and cavitated WAS samples were centrifuged at 13,000*g* before use. A series of molecular weight indices were calculated from the absorption spectra to characterize the chromogenic DOM (cDOM): specific ultraviolet absorbance (SUVA254), specific visible absorbance (SViA420), cDOM index, E255/E355 ratio, E465/E665 ratio, and sum of absorbances (A250-A450). Further, 3D excitation-emission (Ex-Em) spectral profiles (excitation: 230–400 nm (1 nm step) and emission: 400–600 nm (1 nm step)) of fluorogenic organic matter were determined as described before (Helms et al., 2009).

For the characterization of nucleic acids, the following characteristic wavelengths routinely used in DNA analyses were extracted: A230 (aromatic compounds, polysaccharides), A260 (DNA, RNA), A280 (proteins), A320 (chromogenic compounds). The mean ± sd values at each characteristic wavelength and the extent of increase were determined on a sample-by-sample basis, and the DNA purity indices A260/230, A260/280 were calculated to determine the extent of change in the contribution of compounds other than DNA as described before (PROMEGA application note).

Deionized water (Millipore) was used as a negative control in triplicate for all measurements. Multivariate analyses (npMANOVA, nmMDS; $p < 0.05$; Benjamini-Hochberg correction (Benjamini and Hochberg, 1995) for multiple comparisons) were used to test for

Table 1
Experimental conditions for the two investigated HC regimes.

Exp	D_s (mm) × N_s[a]	D_r (mm) × N_r[a]	n (RPM)	Δp (kPa)	P_0 (kPa)	Q (L/s)	P (kW)	Np	V (L)
AB0		Initial, non-cavitated							
A1	12 × 15	16 × 8	2700	102	22	8.0	6.3	15	320
A2								30	
B1		10 × 8	3000	99	26	8.7	6.5	15	320
B2								30	

[a] N_s: number of stator pins, N_r: number of rotor pins.

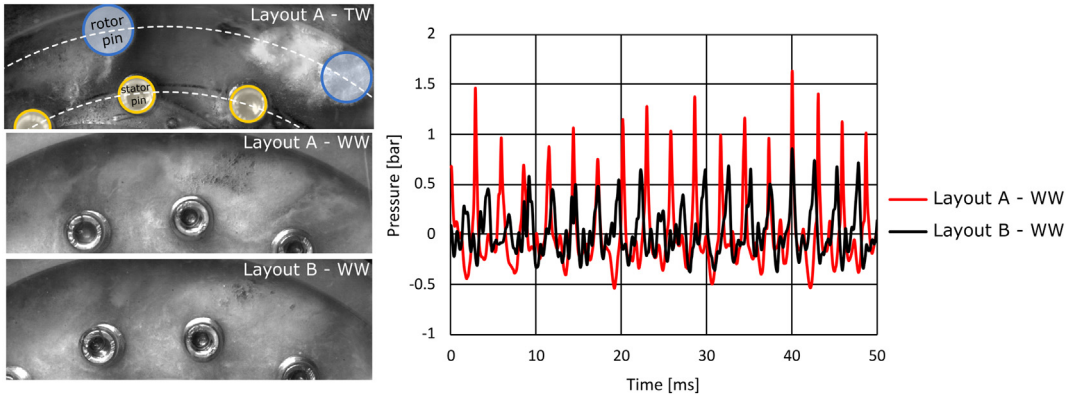

Fig. 3. Example of the occurrence of cavitation in TW and WW for the investigated HC layouts (left images) and corresponding pressure pulsation measurements in WW (right image).

differences between the five samples (non-cavitated and cavitated) and to visualize the results. All measurements were aimed at exploring the general changes in the nature of the chromogenic, fluorogenic and phenolic compounds of DOC as a result of the physical changes and chemical reactions associated with cavitation. Detailed descriptions of the procedures are provided in the Supplementary material., Suppl. 3.

2.3.3. Evaluation of most important WAS contaminants

2.3.3.1. Potentially toxic metals' determination and fractionation analysis. To determine the total PTM content in non-cavitated and cavitated samples, 20 L of each WAS sample was transferred individually to the chamber filter press where solid and liquid phases were separated. The liquid phase was stored at 4 °C until analysis. The solid phase was dried at 40 °C. Pb, Zn, Cu, Mn, and Fe in samples were determined by AAS (Varian, AA240FS) and As and Cr by graphite furnace AAS (GF-AAS, Agilent, 240Z AA) after aqua regia extraction (ISO 1144624, 1995). All analyses were done in triplicate.

The standard Tessier's sequential extraction procedure (Tessier et al., 1979) was used to determine the association of Pb, Zn, Cu, Mn, Fe and Cr with the exchangeable, carbonate, sulfide and Fe, Mn oxide, organic matter, and residual fractions of the sludge.

Analysis of variance (ANOVA) was performed to evaluate the differences between cavitated and non cavitated WAS samples based on the analysed parameters. In case of significant interactions, Duncan's test ($p < 0.05$) was used to test the differences between the mean values. Statistical analysis was performed using R software environment (R Core Team, 2020).

2.3.3.2. Microplastic's extraction procedure and analysis. The following procedure was used for extraction of MP from non-cavitated (AB0) and cavitated samples (A2 and B2). 8 g of the dry WAS sample was mixed with 1 L of sodium dodecyl sulfate (SDS) solution (c = 0.5 g/L) at 50 °C for 24 h to separate MP adhered to organic and inorganic impurities (Simon et al., 2018). The solution was then incubated with a cellulase enzyme (*Trichoderma reesei*) at 50 °C for 72 h, having pH of 4.5. The activity of the enzyme was kept at 12,000 enzyme units/L to completely degrade cellulose fibers originating mainly from toilet paper waste (Johnson et al., 2020). Organic impurities were then removed by oxidation with 30% H_2O_2 in the presence of Fenton's reagent (Fe (II) 0.05 M) in the ratio of 3:1 at 25 °C to catalyze the reaction (Simon et al., 2018). Finally, a density separation was performed with $ZnCl_2$ solution (density of 1.7 g/L) to separate the MP from impurities. The sample was kept in a separatory funnel for 24 h to separate MP from the sample (Lorenz et al., 2019).

MP Fourier transform infrared (FTIR) spectroscopy analyses were performed at room temperature on a Bruker Lumos in attenuated total reflection (ATR) mode using a germanium crystal. The FTIR spectra of the polymers isolated from the WAS samples were recorded in the frequency region of 600 cm^{-1}–4000 cm^{-1}. The FTIR signal was obtained by averaging 64 scans at a resolution of 8 cm^{-1}. Optical microscopy was performed using a LEICA DMS 1000 digital stereo microscope with a coded lens, allowing magnifications up to 300×. A WITec alpha 300 confocal Raman microscope and imaging system was used to measure the Raman spectra of the samples. The microscope was equipped with a thermoelectrically cooled charge-coupled device and a 532-nm laser. The spectra were recorded with a 20× objective and a laser power of 10 mW.

During the experiments no plasticware was used except for colored nitrile rubber gloves and plastic PE wash bottle.

3. Results

3.1. Physical evaluation

3.1.1. Effect of cavitation on particle size and distribution

Physical evaluation of PD RGHC efficiency was performed using particle size and distribution analysis (Table 2). The smallest mean particle size of disintegrated WAS sample was 11.8 μm. The particle size of AB0 ranged from 0.1 to 500 μm with a mean particle size of 98.4 μm. The mean particle size in AB0 was significantly higher compared to the cavitated samples (layout A and B), 98.4 compared to 15.6 and 11.8 μm, respectively. The most common particle size decreased for 90.3% from 131. 2 μm up to 12.7 μm. The percentile particle size d90, d50 and d10 of the treated samples were reduced by 85.4 and 89.8%, 83.9 and 85.8%, 62.0 and 63.4% for layout A and B, respectively. The largest particles were reduced most effectively. The results in both HC regimes (layout A and B) for the studied parameters were similar and longer cavitation times (Np) led to better results in both layouts. The smallest mean particle size and the highest specific surface area were obtained in sample B2 (Table 2). The smallest span value obtained for sample B2, indicates that the particles present in this sample were the smallest.

Table 2
Particle size and percentile before (AB0) and after the two HC treatments (layouts A and B).

	AB0	A1	A2	B1	B2
D[4,3] (μm)	98.4	21.4	15.6	18.2	11.8
mode (μm)	131.2	15.0	13.6	14.5	12.7
median (μm)	87.2	20.1	12.4	13.9	11.0
d10 (μm) [%]	11.2	5.1	4.3	4.7	4.1
d50 (μm) [%]	77.0	15.1	12.4	13.9	11.0
d90 (μm) [%]	210.6	45.1	30.7	37.5	21.5
Specific surface area (cm^2/cm^3)	2.6×10^3	7.5×10^3	8.8×10^3	7.4×10^3	10.4×10^3
Span	2.6	2.7	2.1	2.3	1.6

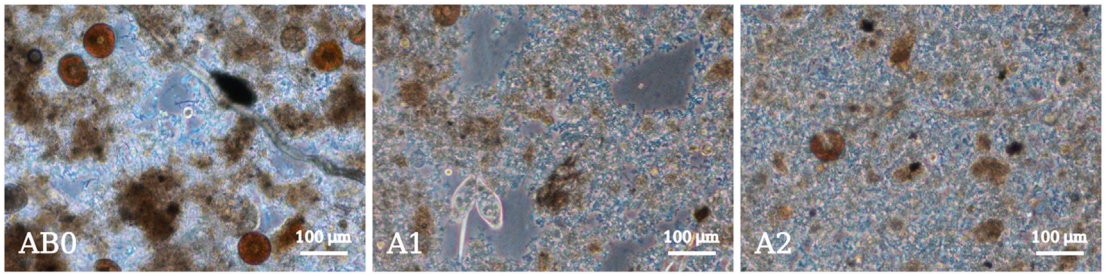

Fig. 4. Microscopic images (100× magnification) of WAS before and after HC treatment (left image - sample AB0, middle image – sample A1 and right image – sample A2).

3.1.2. Effect of cavitation on microorganisms

The disintegration effect of HC on WAS samples was evaluated microscopically. The difference between AB0 and cavitated samples after 15 and 30 Np in floc size, shape and their distribution were observed (Fig. 4). No major differences were observed between the two HC regimes studied so the images in Figs. 4 and 5 represent only the changes observed after 15 and 30 Np.

The image of the initial WAS sample (Fig. 4, left image – sample AB0) shows an abundance of large flocs with empty spaces between the flocs where the microorganisms are not evenly distributed on the surface. After 15 Np (Fig. 4, middle image – sample A1) smaller flocs with better dispersion of microorganisms can be seen. After 30 Np (Fig. 4, right image – sample A2), flocs disintegration was even more pronounced and fewer empty spaces between the flocs can be observed.

The WAS is composed of various microorganisms, such as bacteria, fungi/yeasts, algae, protozoa, helminths, viruses, and other microscopic plants and animals. The most pronounced damage was observed on yeast cells and *Epistilys species*. Different types of damages to yeast cells were present after 15 Np (Fig. 5 - b1, b2, b3), while damage to *Epistilys species* was observed after 30 Np (Fig. 5 – a1). Damaged cell walls and *Epistilys* heads (i.e., peristomial discs) torn off from the stems represented the main mechanical effects of HC on the cells of microorganisms in WAS.

3.2. Chemical evaluation

3.2.1. Effect of cavitation on WAS characteristics

The effect of RGHC on WAS characteristics was evaluated by chemical analyses (Table 3). No differences of WAS characteristics were observed between the two HC regimes (layout A and B). Total solids (16.7 ± 0.6 g/L) and volatile solids (12.4 ± 0.5 g/L) did not change during HC treatment. Similarly, total COD (COD) (16,700 ± 900 mg/L) did not change, while an increase in sCOD was seen, confirming the disintegration and solubilization of WAS (Table 3). This was further supported by increased soluble TOC, NH_4-N and PO_4-*P* values. Soluble NO_x-N values (sum of NO_3-N and NO_2-N) also increased indicating chemical nitrification. There were no differences in the values determined for soluble total nitrogen (146.5 ± 2.1 mg/L), total phosphorus (536.5 ± 4.9 mg/L) and soluble phosphorus (65.5 ± 3.5 mg/L) between non-cavitated in cavitated samples. The results are reported in Supplementary material, Suppl. 1. Linear Pierson correlation confirmed that the release of soluble organic fractions increased with cavitation time (Np). A statistically significant difference was found between sCOD and sTOC of non-cavitated and cavitated samples ($p < 0.05$) and a strong correlation between Np, sCOD and sTOC ($r = 0.974$ and $r = 0.889$, respectively). There are correlations between sCOD, sTOC, NO_x-N, specific surface area and mean size of WAS particles and statistically significant differences between non-cavitated and cavitated samples ($r > 0.88$, $p < 0.05$). Detailed statistical calculations can be found in the Supplementary material, Suppl. 4.

The calculation of DD of WAS (Eq. (3)) was based on the alkaline pre-treatment (Erden and Filibeli, 2010). The values of DD increased with longer Np and the highest values were reached after 30 Np, 7.7 ± 0.6% and 6.0 ± 0.6% for A2 and B2, respectively.

During the experiments, pH decreased from 6.9 in AB0 to 6 and 6.2 in HC layouts A and B, respectively. Conductivity, salinity, and DO (1121 µs/cm, 0.36 ppm and 0.39 mg/L, respectively) did not change

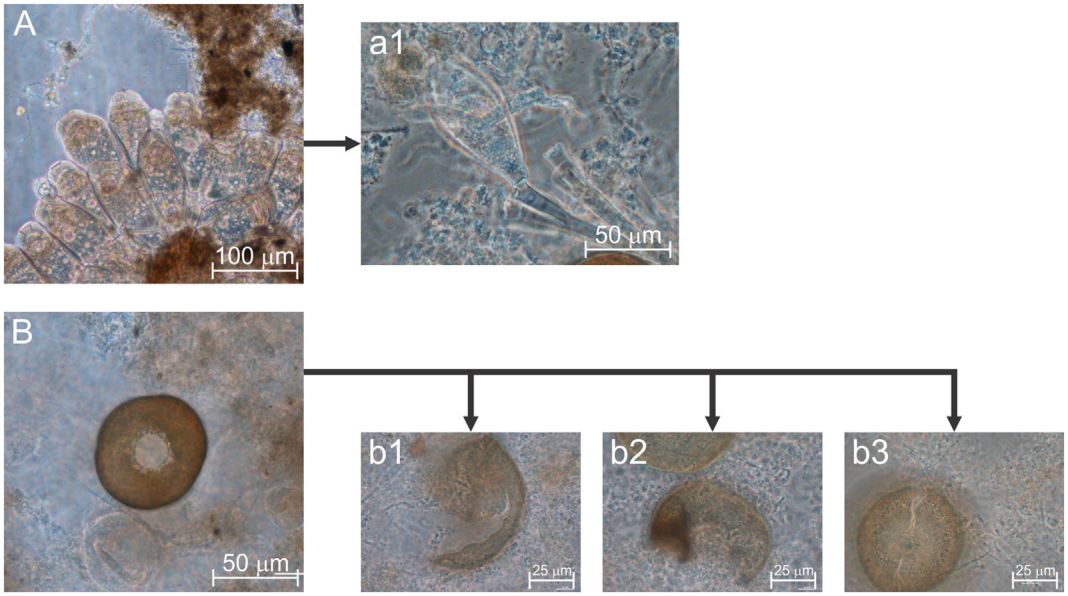

Fig. 5. Images of *Epistylis* sp. (image A) and yeast cells (image B on) in the initial WAS sample (AB0) and the different damages observed after HC treatment (images a1, b1, b2 and b3).

Table 3
WAS characteristics of soluble fractions before (AB0) and after the two HC treatments (layouts A and B).

Exp Par	AB0	A1	A2	B1	B2
sCOD(mg/L)	207 ± 14	345 ± 40	530 ± 1	376 ± 25	459 ± 57
sTOC (mg/L)	292.5 ± 34.6	333.5 ± 26.2	345 ± 11.3	322 ± 4.2	331.5 ± 7.8
NH_4-N (mg/L)	9.5 ± 0.7	21 ± 0.0	21.5 ± 0.7	20 ± 0.0	18.5 ± 0.0
NO_3-N (mg/L)	3 ± 0.7	9.5 ± 0.1	10.5 ± 0.7	9 ± 0.1	9.5 ± 0.7
NO_2-N (mg/L)	0.06 ± 0.01	0.10 ± 0.01	0.11 ± 0.01	0.08 ± 0.01	0.11 ± 0.01
PO_4-P (mg/L)	35 ± 0.3	45.4 ± 1.7	44.1 ± 3.7	43.7 ± 3.4	43.1 ± 3.5
DD (%)	–	3.3 ± 0.4	7.7 ± 0.6	4.0 ± 0.4	6.0 ± 0.6

during the experiments, and temperature increased from 14 °C to 18 °C in both layouts (Supplementary material, Suppl. 1).

3.2.2. Effect of cavitation on microbial DNA and DOM

Aliquots of WAS were used to determine the number of microbial cell equivalents based on the amount of DNA extracted as a rough estimate of cell lysis. Essentially no differences detected in the amount of microbial DNA extracted from 0.25 g WAS aliquots were observed between the initial WAS samples and after cavitation under either HC regime, resulting in comparable estimates of microbial cell density per g WAS (5.76 ± 1.3 10^9 cells/250 mg WAS).

In contrast to the DNA analyses based on WAS, UV-VIS and Ex-Em spectroscopy were used to characterize the chemical nature of the water samples (aromatic, chromogenic and fluorescent compounds) because compounds with low-MW could be released into the water after cell rupture, physical disintegration of cell surface components, and/or additional modifications of chemical structure due to cavitation-mediated chemical reactions.

The UV-VIS spectroscopy results showed that HC itself significantly affected the UV-VIS spectra of the cavitated WAS samples compared to the non-cavitated ones (npMANOVA, $p < 0.10$). In-depth UV-VIS analyses of non-cavitated and cavitated samples, using different indices from the spectral analyses of surface waters showed that due to of cavitation, the MW, chromogenicity, O:C ratio, C:N ratio and carboxyl content of the molecules in the supernatant were increased, while the aromaticity of the dissolved molecules decreased (Supplementary material., Suppl. 5 and 6).

The results show that cavitation significantly increased the abundance of all biologically relevant compounds, regardless of the HC regime studied (Table 4). The fold increase in the contribution of the different compounds to the spectroscopic signal (Table 5) showed increased values of the biologically relevant DOM by 50–77% (A1), 23–44% (A2), 48–58% (B1), 113–128% (B2). The lowest values were observed in sample A2 (Table 5), with still more than 23% increase of various biologically relevant compounds. However, they were half lower than the values obtained in sample A1 (shorter cavitation time), suggesting chemical changes.

The characteristic indices describing which compound contributes more to the signal, were not significantly affected, and remained largely stable (260/230, 260/280, 260/320 and 280/320 were 0.53, 1.13, 1.87 and 1.65, respectively), regardless of the cavitation regime (npMANOVA, $p > 0.05$).

The Ex-Em spectroscopy results confirmed that different chemical changes occurred in response to cavitation depending on the HC regime studied. The results show a gradual increase in the fluorescence of the compounds present in the water after cavitation compared to the AB0 sample for both HC regimes studied (AB0 = 4521 ± 165; A1 = 4672 ± 621; A2 = 8133 ± 613; B1 = 7931 ± 658, B2 = 12,263 ± 164 relative fluorescence units). A more than twofold increase in the emitted fluorescence was seen in the water samples after the initial WAS sample - AB0 (Fig. 6 - image A) was exposed to 30 Np in layout B (Fig. 6 - image B).

3.3. Evaluation of WAS contaminants

3.3.1. Effect of cavitation on potentially toxic metals (PTM)

The EU Directive 86/278/EEC (86/278/EEC) has introduced limits for PTM in WAS to protect human health. Comparison of total concentrations of PTM in the solid part of the initial WAS sample (AB0, Table 6) with the legislation for biosolids used in agriculture, based on the Slovenian legislation (Official Gazette of the Republic of Slovenia: 62/2008), showed that the total contents of Pb and Cr fell within the threshold values for biosolids, while values for Zn and Cu exceeded the permissible standards. The trace elements such as Cu, Zn, Mo, Mn and Fe are essential micronutrients required for plant growth but can become toxic at high concentrations (Parveen et al., 2015). High concentrations of Fe and Mn were also detected in AB0 (Table 6), but these two elements are not regulated by the EU Directive 86/278/EEC (86/278/EEC).

It is evident that the total concentrations of metals were reduced by HC treatment (Table 6). The most drastic decrease in concentration of PTM was observed for Pb: compared with sample AB0, cavitation significantly decreased Pb by 21% in sample A1, 67% in sample A2, 64% in sample B1, and 70% in sample B2 (Table 6). HC significantly decreased also the total Cu content in A1, A2, B1 and B2 by 22%, 28%, 21% and 29%, respectively, compared with AB0 (Table 6). However, the total concentrations of Cu in cavitated WAS samples were still above the limits. The total Zn content in cavitated WAS samples decreased by 28% on average compared with AB0 (Table 6) and was within the thresholds. The HC treatment had no impact on As in sample A1, but decreased As below the detection limit in samples A2, B1 and B2 (Table 6). Total Mn and Cr contents were not significantly reduced by HC, while concentrations of total Fe in samples A1, A2 and B2 were 11–16% lower than in AB0 (Table 6).

Table 4
Mean values of characteristic wavelengths from spectroscopic analyses of water samples before (AB0) and after the two HC treatments (layouts A and B). A230 (aromatic compounds, polysaccharides), A260 (DNA, RNA), A280 (proteins), A320 (chromogenic compounds). Standard deviation <10%.

Exp	Mean values – water background			
	A230	A260	A280	A320
AB0	*0.312*	*0.211*	*0.178*	*0.100*
A1	0.553	0.340	0.289	0.159
A2	0.450	0.268	0.228	0.124
B1	0.494	0.314	0.269	0.151
B2	0.705	0.451	0.387	0.229

Table 5
Fold increase in signal after the two HC treatments (layouts A and B). Standard deviation <10%.

Exp	Fold increase (%)			
	A230	A260	A280	A320
AB0	*1*	*1*	*1*	*1*
A1	1.77	1.61	1.62	1.58
A2	1.44	1.27	1.28	1.23
B1	1.58	1.48	1.51	1.50
B2	2.26	2.13	2.17	2.28

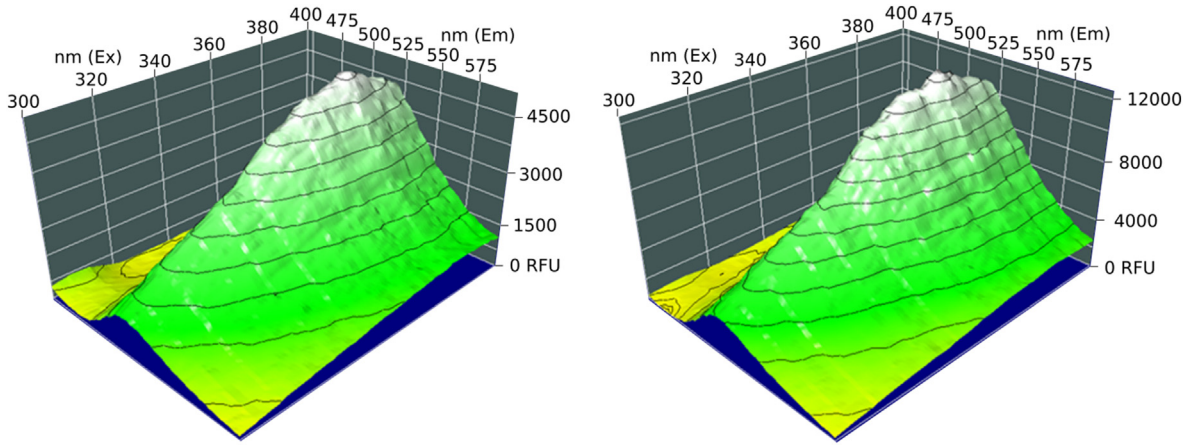

Fig. 6. An example of the Ex-Em spectroscopy results before cavitation and after HC layout B. Image A represents the non-cavitated sample (AB0), while image B represents sample B2.

The PTMs in the liquid part were also analysed. As in the solid part, PTM concentrations in the precipitate of the liquid part of WAS were generally lower in the cavitated samples than in AB0. Detailed results are given in the Supplementary material, Suppl. 7.

The distribution of PTM in AB0 and cavitated WAS samples was also determined (Fig. 7). In AB0, the organic fraction was predominant for all metals (51–96%), followed by the residual fraction for Cr, Fe, Pb and Cu (20, 12, 11 and 2%, respectively), the carbonate-bound fraction for Mn and Zn (28 and 8%, respectively), and bound to Fe and Mn oxide for Mn and Zn (14 and 8%, respectively) (Fig. 7 and Supplementary material, Suppl. 8). In general, HC did not significantly change the distribution of metals in WAS samples (Fig. 7 and Supplementary material, Suppl. 8).

3.3.2. Evaluation of microplastics (MP) present in WAS samples

Following the described procedure, optical microscopy showed MP in all analysed WAS samples: untreated AB0 and cavitated A2 and B2. Optical microscopy showed MP in the range of 100 μm - 1 mm which consisted of colored fragments of unknown origin and fibers likely originating from clothing washing. Typical microfibres (red, orange, blue and yellow) and fragments are shown in the Supplementary Material, Suppl. 9. The number of fibers was much higher than the number of fragments (generally a ratio of 10:1). The concentration of MP particles did not differ significantly among the three WAS samples analysed. A selection of MPs identified by optical microscopy were further analysed by FTIR and Raman spectroscopy to confirm their artificial origin and to determine the type of the material. By comparing the spectra of the particles with spectra in the spectral database, seven MP particles were confirmed by FTIR to be made of synthetic polymers: five consisted of polyethylene (PE), one of polypropylene (PP), and one of polyethylene terephthalate (PET). The FTIR spectra are shown in Fig. 8, left image. Additional FTIR spectra of PE can be found in the Supplementary material, Suppl. 10.

Raman spectroscopy is often used as a complementary technique to FTIR and is particularly advantageous for smaller particles (Araujo et al., 2018). Nine MP were characterized by Raman spectroscopy, including four colored particles and five dark or unpigmented particles. Two were made from PE, two from PP, and three from polyamide. Representative Raman spectra of PE, PP, and polyamide-6 (PA-6) are shown in Fig. 8, right image. Two colored particles (red and pink) showed fluorescence and spectra matching pigment Red 254 (1,4-bis(4-chlorophenyl)-2,5-dihydropyrrolo[3,4-*c*]pyrrole-3,6-dione), which is widely used in the plastics industry. Raman spectra of various MP and red/pink dye can be found in the Supplementary material, Suppl. 11 and Suppl. 12, respectively.

4. Discussion

There are three possible pathways for disintegration of flocs, destruction of microorganisms and organic compounds present in WAS during cavitation: mechanical, chemical, and thermal. Mechanical effects of cavitation result from the collapse of bubbles, which generate high intensity shock waves and hydro-mechanical shear forces in the fluid surrounding the bubbles. These can disintegrate flocs and cause the release of organic matter from the inner part of the flocs, resulting in enhanced WAS solubilization. In addition, they can break intra- and intermolecular bonds, breaking molecules with high MW into lower ones (Wang et al., 2021; Holkar et al., 2019). Furthermore, microjets combined with local shear forces can damage cells of individual microorganisms and release their intracellular matter – biologically relevant DOM. The extreme conditions created by bubble collapse, namely high local temperatures, and pressures, simultaneously cause chemical effects, through homolytic cleavage of water molecules into hydroxyl radicals, that can oxidize soluble organic molecules in WAS. It is postulated that •OH and/or various reactive oxygen species (ROS), formed under different conditions during HC can cause damage to cells of microorganisms, as thoroughly described in Zupanc and co-workers (Zupanc et al., 2019). Additionally, high local temperatures (presumably several 1000 K) (Benito et al., 2005) can thermally degrade and destroy the cell walls of microorganisms present in WAS. During the collapse of the cavities, the gas-liquid mass transfer of the reactants is also enhanced due to the turbulence caused by this collapse (Kim et al., 2020; Wang et al., 2021; Khanal et al., 2007; Holkar et al., 2019).

Table 6
Concentration of PMTs (mg/kg) before (AB0) and after the two HC treatments (A1, A2, B1, B2) in WAS samples (solid part). Average values with standard error (n = 3) are shown. A different letter denotes significant differences (Duncan test, $p < 0.05$).

	Pb (mg/kg)	Zn (mg/kg)	As (mg/kg)	Fe (mg/kg)	Cu (mg/kg)	Mn (mg/kg)	Cr (mg/kg)
AB0	180 ± 7.2 ^{a}	1539.4 ± 9.3 ^{a}	2.9 ± 0.1 ^{a}	48,216 ± 1944 ^{a}	469.5 ± 5.3 ^{a}	332.7 ± 5.1 ^{a}	108.9 ± 0.7 ^{a}
A1	142.1 ± 0.6 ^{b}	1092.4 ± 15.1 ^{b}	3.3 ± 0.2 ^{a}	40,528 ± 641 ^{b}	365.7 ± 2.0 ^{b}	317.8 ± 3.4 ^{ab}	112 ± 1.2 ^{a}
A2	59.6 ± 3.7 ^{c}	1092.4 ± 18.5 ^{b}	n.d.	42,921 ± 463 ^{bc}	338.6 ± 1.0 ^{c}	308.2 ± 1.3 ^{b}	106.7 ± 1.1 ^{a}
B1	65.7 ± 1.5 ^{c}	1168.2 ± 21.9 ^{c}	n.d.	44,523 ± 141 ^{ac}	368.8 ± 4.2 ^{b}	317.1 ± 3.9 ^{ab}	122.2 ± 1.7 ^{a}
B2	54.1 ± 0.7 ^{c}	1076.0 ± 29.5 ^{b}	n.d.	40,545 ± 1565 ^{b}	335.4 ± 8.5 ^{c}	292.8 ± 8.0 ^{c}	107.0 ± 1.8 ^{a}

n.d. = not detected.

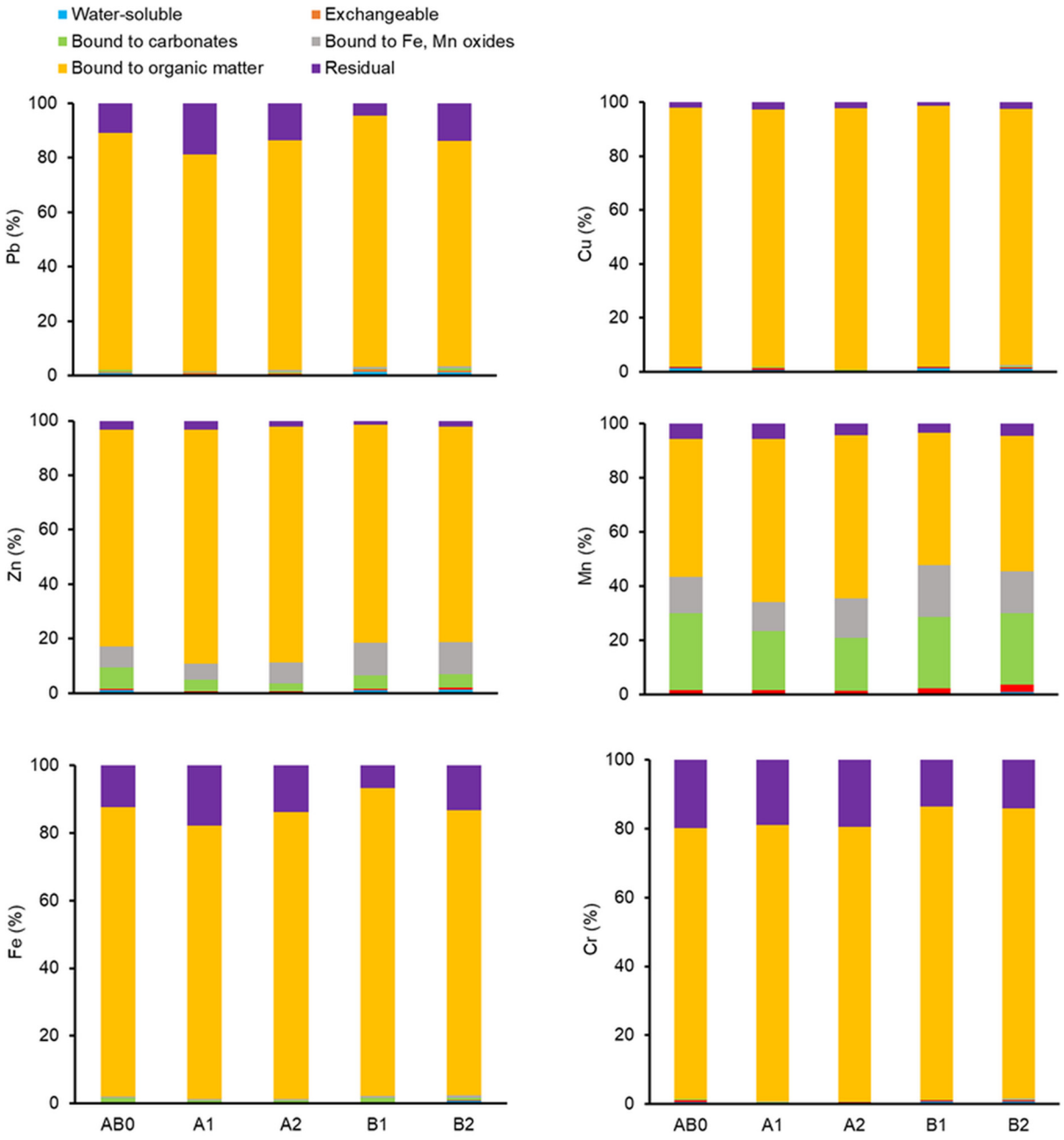

Fig. 7. Metal fractionation before (AB0) and after the two HC treatments (layouts A and B) in WAS samples. Data are given as an average of 3 combined samples.

The mechanical effects of PD RGHC were first determined by physical evaluation of the samples. The disintegration ability of PD RGHC was confirmed while no differences were found between the two HC regimes. The mechanical effects resulted in reduced floc size, decreased mean particle size, and increased specific surface area for all cavitated WAS samples (Table 2). It can be observed that the volume occupied by small particles increased with cavitation time (Table 2: D[3,4], d90, d50, d10). The largest particle size reduction (88%) and specific surface area increase (300%) compared to AB0, was obtained in RGHC layout B (Table 2, sample B2). With longer Np, statistically significant differences and strong correlations were observed between the specific surface area of non-cavitated and cavitated samples ($r = 0.952$, $p < 0.05$). Strong inverse correlations between non-cavitated and cavitated samples were observed between N_p and mean particle size ($r = -0.848$). Detailed statistical calculation can be found in Supplementary material, Suppl. 4. A similar particle size reduction of 79% and 82% under optimized HC conditions was reported by Kim and co-workers (Kim et al., 2020) and Cai and co-workers (Cai et al., 2018), respectively. The mechanical effects were also confirmed by microscopic images of floc disintegration (Fig. 4). The disintegration of flocs by HC has also been observed in other available studies, either in the form of particle size and distribution analysis (Kim et al., 2020; Cai et al., 2018) or microscopic images (Petkovšek et al., 2015; Cai et al., 2018).

The mechanical effects of PD RGHC extend to the observed damage to the cells of individual microorganisms (Fig. 5). The mechanism of destruction observed on a yeast cell (Fig. 5 – images b1 and b2) can most likely be associated with the impact of the microjet resulting from bubble collapse (Dular et al., 2019). An indirect impact "peels" the cell (Fig. 5 – image b1), while a direct impact splits it in half (Fig. 5 – image b2). Even more interesting is the case shown in Fig. 5 – image b3, where the damage is concentrated on the "poles" of the yeast cell. Relating the specifics of this case to the recent simulations of the bubble

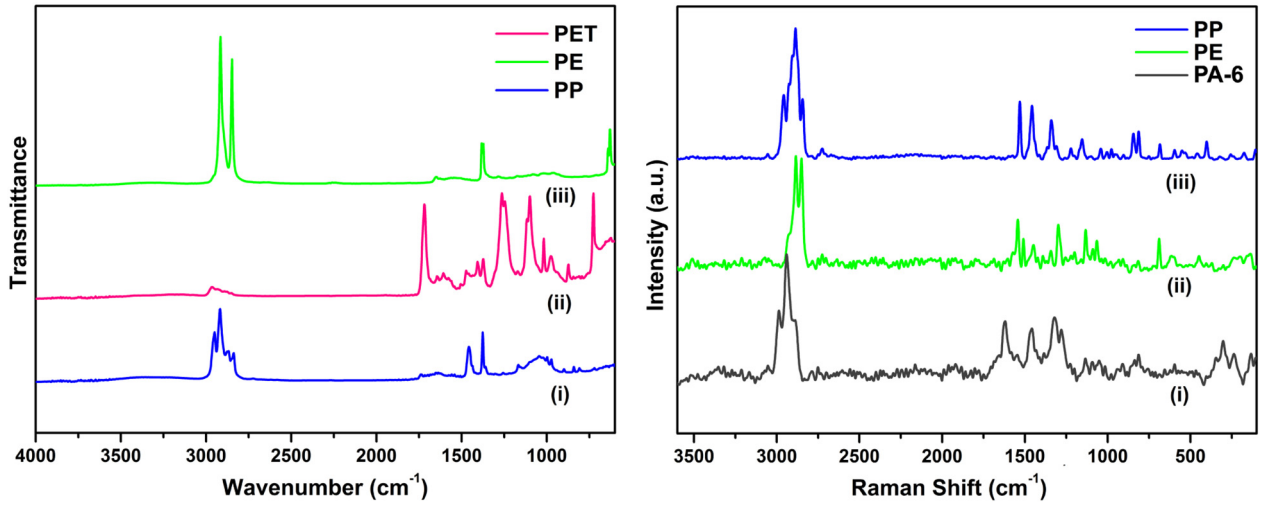

Fig. 8. Left image: FTIR spectra of particles isolated from WAS samples: i) polypropylene (PP), ii) polyethylene terephthalate (PET), and iii) polyethylene (PE); Right image: Raman spectra of various MP: polyethylene PE (i), polyamide- 6 (PA-6) (ii), (iii) and polypropylene PP (iv).

- liposome interaction (Zevnik and Dular, 2020), two other possible mechanisms emerge: (i) local wrinkling at the cell pole until the bubble rebounds, and (ii) stretching at the pole of the structure during the phase of a second bubble contraction. Furthermore, Fig. 5 – image a1 shows "decapitated" *Epistylis* sp. (an intact one is shown in Fig. 5 – image A). Again, the mechanism of damage can be attributed to bubble collapse and the resulting effects - such as microjet impact and local shear forces resulting from the fast-moving fluid flow during bubble evolution. The mechanical damage observed to yeast cells after various cavitation treatments has been described in detail elsewhere in the literature (Zupanc et al., 2019). Despite the observed ruptures in the cell walls (Fig. 5 – images b1, b2, b3), the results of microbial DNA extraction coupled with spectroscopy analyses of the water samples showed that the intracellular high-MW DNA did not leak from the cells (see Section 3.2.2). Furthermore, the extent of ruptured cells observed microscopically (Fig. 5) suggests that the viability of these cells was significantly affected, however, based on DNA extraction, their DNA was not completely released into the surrounding water, and was apparently only slightly broken down into smaller MW DNA fragments. Additionally, these results indicate that cavitation did not induce selective degradation of specific organic compounds or complexes present in WAS nor did it result in a significant increase in DNA released from microbial cells, but it affected EPS and sludge particle surfaces, composed of extracellular DNA, polysaccharides, and proteins. The extracellular DNA released from EPS in water as measured by spectroscopy (when converted to corresponding cell equivalents for simplicity), was equivalent to $4.2 \cdot 10^3$–10^4 microbial cell equivalents per 100 uL in terms of DNA content (2.5–5.7 · 10^6 cells/60 mL). This extracellular pool of DNA released from EPS is three orders of magnitude smaller compared to the actual cellular DNA pool extracted from the initial WAS samples, which corresponded to 10^9 cells per 250 mg of sludge, concentrated from 60 mL of water.

The evaluation of mechanical pre-treatment methods for WAS disintegration is based on DD. Comparing the values of DD reported in the literature is difficult for several reasons. First, the calculations of DD differ depending on how $sCOD_{max}$ is determined in Eq. (3), and authors choose this value differently. $sCOD_{max}$ can thus be represented as sCOD obtained upon chemical disintegration with NaOH (Khanal et al., 2007; Erden and Filibeli, 2010) or H_2SO_4 (Petkovšek et al., 2015). While some authors even use the total COD as the maximum value of sCOD (Vilarroig et al., 2020; Lee and Han, 2013). Secondly, there is not much data for the use of HC for WAS disintegration at pilot-scale. For these reasons, the comparison of DD values reported in the available literature is very difficult. However, the values from a few representative pilot-scale studies, range from 3.3–58% (Table 7). The maximum DD achieved in this study fits within this range and was 7.7 ± 0.6% (Table 3).

Second, the mechanical effects of RGHC were additionally supported by the chemical evaluation. Again, as in the physical evaluation no differences were found between the two HC regimes studied. The increased MW, chromogenicity, O:C ratio, C:N ratio and carboxyl content of the molecules in the supernatant (Supplementary material, Suppl. 5) are illustrated by the results in Table 3. It can be seen that sCOD and sTOC increase with Np in both HC regimes studied, indicating the release of EPS due to floc disintegration (Fig. 4) and the release of

Table 7
Comparison of cavitation/energy efficiency parameters obtained from different studies.

Study	Method/setup	sCOD (mg/L)	TS (g/L)	V (L)	DD (%)	DR (%/h)	P (kW)	t (min)	SE (kJ/kgTS)	SESS (kJ/g sCOD)
Present	PD RGHC A2 (pilot-scale)	207 ± 14	16.7	320	7.7[a] ± 0.6	23.1 ± 1.2	6.3	20	$1.41 \cdot 10^3 \pm 0.16 \cdot 10^3$	73 ± 2
	PD RGHC B2 (pilot-scale)				6.0[a] ± 0.6	19.6 ± 1.2	6.5	18.4	$1.34 \cdot 10^3 \pm 0.1 \cdot 10^3$	89 ± 4
(Vilarroig et al., 2020)	SD RGHC (lab-scale, best)	76 ± 35	7.2	40	26.0[b]	52.0	5.7	30	$3.58 \cdot 10^4$	271
	SD RGHC (pilot-scale, avg)	6320 ± 1950	55	500	10.1[b]	2.5	6.9	240	$3.63 \cdot 10^3$	57
	SD RGHC (pilot-scale, best)		70	500	17.4[b]	4.4	6.9	240	$2.85 \cdot 10^3$	16
(Petkovšek et al., 2015)	SD RGHC (pilot-scale)	45	10	196	58.0[c]	63.3	5.8	55	$9.77 \cdot 10^4$	175
(Lee and Han, 2013)	Orifice plate (lab-scale)	15 ± 5	9.9	1.5	20.3[b]	60.9	1.5	20	$1.22 \cdot 10^5$	503

[a] Calculated by alkaline NaOH treatment.
[b] Calculated by using total COD.
[c] Calculated by acid H_2SO_4 treatment.

intracellular contents of single cells after breaking the cell walls (Fig. 5). However, the characteristics of WAS depend on the composition of the incoming WW, the biological process, and the plant design (Christensen et al., 2015). Therefore, there are large differences between the COD and sCOD values measured in different WWTPs, which are reported in the literature with values ranging from 1800 to 95,133 mg/L and 15–6320 mg/L for COD and sCOD, respectively (Supplementary material, Suppl. 13 and 14). The determined COD and sCOD values in the AB0 sample (Table 3) were within the range of these values. Because of these discrepancies, comparing the effectiveness of different studies using the same mechanical pre-treatment methods is very difficult. However, the sCOD increase of 2.6× and 2.2× for layout A and B, respectively, obtained in our study (Table 3) is in agreement with the results reported by Kim and co-workers and Garlicka and co-workers (Kim et al., 2020; Garlicka and Zubrowska-Sudol, 2020), while Petkovšek and co-workers (Petkovšek et al., 2015) obtained a 13× increase in sCOD under optimal HC conditions.

To further substantiate the disintegration ability of the two PD RGHC regimes, various parameters of the soluble fractions (NH_4-N, PO_4-P, NO_3-N) were also measured. NH_4-N and PO_4-P levels increased during both HC regimes, confirming the release of extra- and intracellular substances. Increased levels of NO_x-N in all WAS samples could be related to the oxidation of NH_4-N by ROS formed during HC.On one hand Patil and co-workers (Patil et al., 2021), postulated that the removal of NH_4-N in real WW samples takes place via formation of NO_x-N species. On the other hand, Zupanc and co-workers (Zupanc et al., 2014) assumed that HC/H_2O_2 process led to formation of NO_3-N from organic N due to the extreme conditions developed during HC experiments. Since NH_4-N levels increased along with NO_x-N in this study, it could be that NH_4-N released from the flocs/cells was simultaneously transformed to NO_x-N. The levels of sTN and sTP did not change during the two HC regimes studied, which was expected, since the much more aggressive laboratory treatment with the ultrasound probe and the uncontrolled temperature increase during the treatment lead to the same results (Kolbl et al., 2016).

Chemical effects of HC may be the result of the action of various ROS, predominately •OH formed during cavitation. There are studies available reporting on •OH formation during HC in a Venturi constriction (Arrojo et al., 2007; Zupanc et al., 2020).There are however studies missing regarding the concentration of •OH formed during experiments performed in various RGHC devices and the formation of •OH is usually determined only indirectly (Gostiša et al., 2021a; Gostiša et al., 2021b). Similarly, the chemical effects of the PD RGHC were determined only indirectly during this study, however they were confirmed for both HC regimes studied and are shown via the UV-VIS analyses. The results showed that the aromaticity of the dissolved molecules decreased (Supplementary material, Suppl. 5), indicating either the release of new compounds and/or the chemical modification of the existing molecules in the water after cavitation. Additionally, Ex-Em spectroscopy results confirm that various chemical changes occurred in response to cavitation, as significantly increased fluorescence was observed after cavitation (Fig. 6). The release of cell contents from broken cells, such as proteins and their disintegration can result in fluorescence signal of the amino acids tryptophan, tyrosine, and phenylalanine. This fluorescent signal is further complemented by the release of compounds from EPS upon disintegration, such as aromatic compounds, including extracellular DNA. Free DNA is generally part of EPS as it is released during cell lysis and/or secreted by active cells (eDNA) (Sheng et al., 2010). The overall increase in fluorescence in WAS samples after HC treatment supports the observation that the chemical nature of the compounds present in the supernatant was altered by cavitation. More detailed characterization of the chemical changes that occur during cavitation would require analysis of the samples using GS-MS/MS.

Since WWTPs are considered a critical source of various contaminants, such as PTM and MP, we additionally evaluated the impact of PD RGHC on PTM, while in the case of MP, which is present in WAS, only a determination and identification analysis were performed.

When comparing the cavitation treatments (A1-B2) with non-cavitated sample (AB0), 30 Np in both cavitation regimes A and B, resulted in the lowest content of metals (WAS samples A2 and B2), especially in the second cavitation regime (WAS sample B2, Table 6). In a study investigating the potential of ultrasound-activated persulfate oxidation as a method for enhancing WAS dewaterability, Bian and co-workers (Bian et al., 2021) also found reduced levels of As, Cd, Cu, Ni and Zn (up to 59%) in the treated sludge cake compared to the raw sludge, due to transformation from the insoluble to the soluble state. Compared with AB0, the reduction of As, Fe and Mn in the cavitated WAS samples in our study was insignificant (Table 6). Conversely, our results show that Pb, Zn and Cu were lost during cavitation (Table 6). It remains unclear why the total concentrations of Zn, Cu and especially Pb were reduced after cavitation. The most probable explanation for all three elements is the adsorption of Pb, Zn and Cu with struvite ($MgNH_4PO_4 \times 6H_2O$), which is known to precipitate by cavitation in WWTP (Perwitasari et al., 2018), (Lee et al., 2019). The most drastic reduction was observed for Pb, which could also co-precipitate with Fe-hydroxides (Dai and Hu, 2015), due to the high Fe concentrations (Table 6), as the sludge was treated with $FeCl_3$ (for flocculation). However, we did not detect any evidence of precipitated material in the RGHC. Moreover, the concentrations of PTM in the precipitate of the liquid part of the sludge after separation were generally lower in cavitated WAS samples than in AB0 (Supplementary material, Suppl. 7). Cavitation increases the amount of free radicals, which can increase the level of ROS (Kumar, 2011) and oxidize exposed stainless-steel (Fe) surfaces of RGHC. Another very possible reason for the removal of Pb from the sludge was therefore the adsorption of Pb into newly formed Fe oxide-hydroxide surface layer. After adsorption, the Fe core probably provided a reducing power for the immobilization of adsorbed Pb. Due to this dual property of adsorption and reduction, Fe can sequester toxic metals such as Pb with higher standard redox potential (Pb2+/Pb0, E0h −0.13 V) than Fe (Fe2+/Fe0, E0h = −0.44 V) (Mu et al., 2017).

Determination of the total content of PTMs does not provide useful information on the bioavailability, mobility, and behaviour of metals in the environment. The fate of metals in sludge after landfilling depends on the metal content in the sludge and soil properties, which are known to affect the mobility of metals (Ščančar et al., 2001). PTMs introduced into the with the sewage sludge may change their form but remain in available and extractable form for years (Berrow and Burridge, 1990). Therefore, it is important to determine the mobility of metals in sludge before the land disposal. Bian and co-workers (Bian et al., 2021) reported that ultrasound-activated persulfate oxidation increased the exchangeable fraction of Zn and thus its mobility and bioavailability but decreased the mobility of Ni compared to the raw sludge. In contrast, our results showed that cavitation did not significantly change the distribution of metals mainly bound to the organic fraction compared to AB0 (Fig. 7).

Moreover, along with PTM also MP particles and fibers are accumulated in WAS. The presence of MP particles and fibers was confirmed in both cavitated and non-cavitated WAS samples. The applied enzymatic-oxidative purification approach coupled with FTIR, and Raman analysis allowed the identification of four plastics, namely PE, PP, PET, and PA-6. Fibers were more numerous than other MP particles (fragments). These results, both by material and form, are in agreement with literature reports (Iyare et al., 2020; Murphy et al., 2016). Isolation of MP from the WAS sample is challenging, especially when attempting quantitative isolation and going toward the lower size limit (e.g., below 1 μm or at the nanoscale). Mitrano and co-workers (Mitrano et al., 2019) concluded in their study that more than 98% of the nano plastic remains in the sludge and cannot be extracted using the MP extraction techniques developed so far. Another challenge is the detection of high-density MP such as rubber from tire wear and paint particles. Further development of isolation and characterization techniques will be required to accurately identify these particles that can reasonably be expected in WAS.

Cavitation affects the isolation of MP, as WAS is homogenized, and the treated material has a different consistency. We could not confirm any effect of cavitation on MP particles. There were no discernible differences in size, surface morphology or spectra, although the number of particles may be too small to draw a general conclusion. However, cavitation has the effect of dislodging MP particles from the remaining WAS mass, reducing the need for the first step in the isolation process – the use of SDS – which is used to remove impurities adhered to MP particles. In our case, we applied the procedure to treated and untreated samples to remain consistent in the approach. Detaching MP from other materials may support selective removal of MPs from WAS to improve the acceptability of WAS for land applications and reduce the potential for further spread of MP in the environment. Further studies that focus directly on the effect of cavitation on MP in WAS, as well as studies of model systems with MPs only, are needed to confirm these conclusions.

Although we expected, based on the results presented in Fig. 3, that there would be some differences between the two chosen HC regimes (layout A and B), as indicated by the results of pressure fluctuations, the results of the chemical and physical evaluation did not confirm this. Therefore, we performed another comparison between layout A and B based on energy consumption calculations after 30 Np. The results in Table 7 show that layout A (16-mm pins rotating at 2700 RPM) is characterized by lower SESS and higher DR compared to layout B (10-mm pins rotating at 3000 RPM). Again, there is a lack of studies on WAS disintegration on pilot configurations, making it difficult to compare energy consumption between different studies. Large divergences between input parameters (TS, sCOD, COD) further complicate a realistic comparison between different studies. Due to the lack of specified cavitation parameters needed for these calculations, we selected only a few available studies where a comparison was possible. An important observation that emerges from Table 7 is that regardless of the method of cavitation generation, pilot-scale devices significantly outperform the smaller capacity laboratory scale devices in terms of SESS, although the laboratory devices tend to have a higher DR. Vilarroig and co-workers (Vilarroig et al., 2020) reported SESS of only 16 kJ/g of sCOD released for their best industrial case. However, the operating conditions used for this calculation are very different from the experimental conditions used in our study, especially due to the much higher operating temperatures (up to 75 °C). Moreover, the present study PD RGHC showed similar performance to the average performance of SD RGHC studied by Vilarroig and co-workers (Vilarroig et al., 2020) with respect to SESS but our DR was larger by almost an order of magnitude. Apart from the studies shown in Table 7, Kim and co-workers (Kim et al., 2019) also investigated the sludge disintegration performance (dimpled rotor was used as cavitation device) and obtained DD = 18.5% after 26.25 min (5 WAS passes), which corresponds to DR = 42.3%/h for the optimal WAS disintegration case.

The search of the available literature using HC devices at laboratory or pilot-scale revealed large discrepancies in the initial WAS characteristics, that affect the efficiency of the treatments studied and complicate the comparison of disintegration and solubilization effects. Large discrepancies in the calculation of DD further complicate meaningful comparison between different studies. If the authors would systematically report on all important hydrodynamic cavitation parameters (sample volume, flow rate, treatment time, number of treatment passes, energy input and temperature during treatment) and describe experimental conditions in detail, the comparison between studies would be facilitated and optimized, versatile and economically feasible WAS pretreatment methods could be developed more quickly.

5. Conclusions

The present study represents one of the few pilot-scale studies on the disintegration and solubilization of waste activated sludge, where a thorough analysis confirmed the effectiveness of a novel hydrodynamic cavitation generator as a mechanical pre-treatment method. The results of the study showed the presence of mechanical and chemical effects of cavitation. The mechanical effects were reflected by a decrease in mean particle size, an increase in specific surface area, and an increase in sCOD and NH_4-N concentrations. The chemical effects were confirmed by decreased total concentrations of most of the studied metals in the solid part of WAS (most pronounced in the case of Pb), as well as by decreased aromaticity and increased fluorescence of biologically relevant DOM. Our results showed that cavitation has the potential to reduce the total concentration of PTMs in WAS. However, the Cu content still exceeded the limits for agricultural use. Therefore, for use in agricultural soils, WAS should be additionally treated (remediated) to reduce PTM concentrations. In addition, three different types of damage to yeast cells and *Epistylis species* were observed and attributed to microjets and local shear forces. Despite this observed damage, no microbial DNA leaked from the cells, while the amount of biologically relevant DOM increased. Analysis of microplastics confirmed the presence of four different microplastic compounds (PE, PP, PET and PA -6). Contrary to the initial hypothesis, no major differences in impacts were found between the two selected HC regimes, except for energy efficiency. The observations and explanations made in this study can serve as a basis for all future detailed studies of the specific effects of HC on municipal waste sludge (mechanisms of cell disruption, chemical changes of DOM and effects on potentially toxic metals).

CRediT authorship contribution statement

S. Kolbl Repinc: conceptualization, sludge characteristics analysis, writing; **B. Bizjan**: HC characteristics and effects analysis, writing; **V. Budhiraja**: microplastics analysis, writing; **M. Dular**: explanation of HC effects, writing and review; **J. Gostiša**: HC device design, HC characteristics analysis, writing; **B. Brajer Humar**: microscopic analysis, writing; **A. Kaurin**: PTM analysis, writing; **A. Kržan**: microplastics analysis, writing and review; **M. Levstek**: organization of WWTP experiments, writing and review; **J. F. Morales Arteaga**: PTM analysis, writing; **M. Petkovšek**: explanation of HC effects, writing; **G. Rak**: sludge characteristics analysis, writing; **B. Stres**: microbial DNA and DOM analysis, writing; **B. Širok**: development and HC design, writing and review; **E. Žagar**: microplastics analysis, writing and review; **M. Zupanc**: conceptualization, writing and review.

Declaration of competing interest

The authors declare that they have no known competing financial interests or personal relationships that could have appeared to influence the work reported in this paper.

Acknowledgements

The authors would like to acknowledge that this project has been co-financed by the Slovenian Research Agency (core funding nos. P2-0401 and P2-0180 and grant nos. J7-2601 and J7-1814), the Horizon 2020 research and innovation program of the European Union under Marie Sklodowska-Curie (grant agreement no. 860720), the European Network for the Promotion of Portable, Affordable, and Simple Analytical Platforms – COST Action CA16215 and the European Research Council (ERC) under European Union's Framework Program for Research and Innovation, Horizon 2020 (Grant Agreement No. 771567 — CABUM).

The authors would also like to thank Petrol d.d. and the Domžale-Kamnik WWTP for their support. The authors would like to thank Prof. Dr. Ivan Jerman, Nigel Van de Velde, National Institute of Chemistry for providing the Raman Spectroscopy facility. Furthermore, the authors would like to thank the University of Ljubljana for its financial support within the UL Innovation Fund and the support of the UL Knowledge Transfer Office patenting the cavitation device presented in this work (application number: P50434LU00).

Appendix A. Supplementary data

Supplementary data to this article can be found online at https://doi.org/10.1016/j.scitotenv.2021.151414.

References

86/278/EEC, 1986. Directive 86/278/EEC on the protection of the environment, and in particular of the soil, when sewage sludge is used in agriculture, OJ L 181, pp. 6–12 1986.

Ali, H., Khan, E., Ilahi, I., 2019. Environmental chemistry and ecotoxicology of hazardous heavy metals: environmental persistence, toxicity, and bioaccumulation. J. Chem. 2019. https://doi.org/10.1155/2019/6730305.

Araujo, C.F., Nolasco, M.M., Ribeiro, A.M.P., Ribeiro-Claro, P.J.A., 2018. Water Res. 142, 426–440. https://doi.org/10.1016/j.watres.2018.05.060.

Arrojo, S., Nerín, C., Benito, Y., 2007. Application of salicylic acid dosimetry to evaluate hydrodynamic cavitation as an advanced oxidation process. Ultrason. Sonochem. 14, 343–349. https://doi.org/10.1016/j.ultsonch.2006.06.007.

Benito, Y., Arrojo, S., Hauke, G., Vidal, P., 2005. Hydrodynamic cavitation as a low-cost AOP for wastewater treatment: preliminary results and a new design approach. WIT Trans. Ecol. Environ. 80, 495–503.

Benjamini, Y., Hochberg, Y., 1995. Controlling the false discovery rate: a practical and powerful approach to multiple testing. J. R. Stat. Soc. Ser. B 57, 289–300.

Berrow, M.L., Burridge, J.C., 1990. Persistence of metal residues in sewage sludge treated soils over seventeen years. Int. J. Environ. Anal. Chem. 39, 173–177. https://doi.org/10.1080/03067319008027694.

Bhat, A.P., Gogate, P.R., 2021. Cavitation-based pre-treatment of wastewater and waste sludge for improvement in the performance of biological processes: a review. J. Environ. Chem. Eng. 9, 104743. https://doi.org/10.1016/j.jece.2020.104743.

Bian, C., Ge, D., Wang, G., Dong, Y., Li, W., Zhu, N., Yuan, H., 2021. Enhancement of waste activated sludge dewaterability by ultrasound-activated persulfate oxidation: operation condition, sludge properties, and mechanisms. Chemosphere 262, 128385. https://doi.org/10.1016/j.chemosphere.2020.128385.

Cai, M., Hu, J., Lian, G., Xiao, R., Song, Z., Jin, M., Dong, C., Wang, Q., Luo, D., Wei, Z., 2018. Synergetic pretreatment of waste activated sludge by hydrodynamic cavitation combined with Fenton reaction for enhanced dewatering. Ultrason. Sonochem. 42, 609–618. https://doi.org/10.1016/j.ultsonch.2017.11.046.

Carrère, H., Dumas, C., Battimelli, A., Batstone, D.J., Delgenès, J.P., Steyer, J.P., Ferrer, I., 2010. Pretreatment methods to improve sludge anaerobic degradability: a review. J. Hazard. Mater. 183, 1–15. https://doi.org/10.1016/j.jhazmat.2010.06.129.

Christensen, M.L., Keiding, K., Nielsen, P.H., Jørgensen, M.K., 2015. Dewatering in biological wastewater treatment: a review. Water Res. 82. https://doi.org/10.1016/j.watres.2015.04.019.

Collivignarelli, M.C., Abbà, A., Frattarola, A., Miino, M.C., Padovani, S., Katsoyiannis, I., Torretta, V., 2019. Legislation for the reuse of biosolids on agricultural land in Europe: overview. 11, 1–22. https://doi.org/10.3390/su11216015.

Dai, C., Hu, Y., 2015. Fe(III) hydroxide nucleation and growth on quartz in the presence of Cu(II), Pb(II), and Cr(III): metal hydrolysis and adsorption. Environ. Sci. Technol. 49, 292–300. https://doi.org/10.1021/es504140k.

Dular, M., Požar, T., Zevnik, J., Petkovšek, R., 2019. High speed observation of damage created by a collapse of a single cavitation bubble. Wear 418–419, 13–23. https://doi.org/10.1016/j.wear.2018.11.004.

Erden, G., Filibeli, A., 2010. Ultrasonic pre-treatment of biological sludge: consequences for disintegration, anaerobic biodegradability, and filterability. J. Chem. Technol. Biotechnol. 85, 145–150. https://doi.org/10.1002/jctb.2298.

Garlicka, A., Zubrowska-Sudol, M., 2020. Effect of hydrodynamic disintegration on the solubilisation and bioavailability of thickened excess sludge. Ultrason. Sonochem. 64, 105015. https://doi.org/10.1016/j.ultsonch.2020.105015.

Geng, H., Xu, Y., Zheng, L., Gong, H., Dai, L., Dai, X., 2020. An overview of removing heavy metals from sewage sludge: achievements and perspectives. Environ. Pollut. 266, 115375. https://doi.org/10.1016/j.envpol.2020.115375.

Gostiša, J., Širok, B., Repinc, S.K., Levstek, M., Stražar, M., Bizjan, B., Zupanc, M., 2021a. Performance evaluation of a novel pilot-scale pinned disc rotating generator of hydrodynamic cavitation. Ultrason. Sonochem. 72. https://doi.org/10.1016/j.ultsonch.2020.105431.

Gostiša, J., Zupanc, M., Dular, M., Širok, B., Levstek, M., Bizjan, B., 2021b. Investigation into cavitational intensity and COD reduction performance of the pinned disc reactor with various rotor- stator arrangements. Ultrason. Sonochem. 105669. https://doi.org/10.1016/j.ultsonch.2021.105669.

Helms, J.R., Stubbins, A., Ritchie, J.D., Minor, E.C., Kieber, D.J., Mopper, K., 2009. Erratum: absorption spectral slopes and slope ratios as indicators of molecular weight, source, and photobleaching of chromophoric dissolved organic matter (limnology and oceanography 53 955–969). Limnol. Oceanogr. 54, 1023. https://doi.org/10.4319/lo.2009.54.3.1023.

Holkar, C.R., Jadhav, A.J., Pinjari, D.V., Pandit, A.B., 2019. Cavitationally driven transformations: a technique of process intensification. Ind. Eng. Chem. Res. 58, 5797–5819. https://doi.org/10.1021/acs.iecr.8b04524.

ISO 1144624, 1995. Soil Quality – Extraction of Trace Elements Soluble in Aqua Regia. International Organization for Standardization, Genève, Switzerland.

Iyare, P.U., Ouki, S.K., Bond, T., 2020. Microplastics removal in wastewater treatment plants: a critical review. Environ. Sci. Water Res. Technol. 6, 2664–2675. https://doi.org/10.1039/d0ew00397b.

Johnson, A.C., Ball, H., Cross, R., Horton, A.A., Jürgens, M.D., Read, D.S., Vollertsen, J., Svendsen, C., 2020. Identification and quantification of microplastics in potable water and their sources within water treatment works in England and Wales. Environ. Sci. Technol. 54, 12326–12334. https://doi.org/10.1021/acs.est.0c03211.

Khanal, S.K., Grewell, D., Sung, S., Van Leeuwen, J., 2007. Ultrasound applications in wastewater sludge pretreatment: a review. Crit. Rev. Environ. Sci. Technol. 37, 277–313. https://doi.org/10.1080/10643380600860249.

Khanh Nguyen, V., Kumar Chaudhary, D., Hari Dahal, R., Hoang Trinh, N., Kim, J., Chang, S.W., Hong, Y., Duc La, D., Nguyen, X.C., Hao Ngo, H., Chung, W.J., Nguyen, D.D., 2021. Review on pretreatment techniques to improve anaerobic digestion of sewage sludge. Fuel 285, 119105. https://doi.org/10.1016/j.fuel.2020.119105.

Kim, H., Sun, X., Koo, B., Yoon, J.Y., 2019. Experimental investigation of sludge treatment using a rotor-stator type hydrodynamic cavitation reactor and an ultrasonic bath. Processes 7. https://doi.org/10.3390/pr7110790.

Kim, H., Koo, B., Sun, X., Yoon, J.Y., 2020. Investigation of sludge disintegration using rotor-stator type hydrodynamic cavitation reactor. Sep. Purif. Technol. 240, 116636. https://doi.org/10.1016/j.seppur.2020.116636.

Kisser, J., Wirth, M., De Gusseme, B., Van Eekert, M., Zeeman, G., Schoenborn, A., Vinnerås, B., Finger, D.C., Kolbl Repinc, S., Bulc, T.G., Bani, A., Pavlova, D., Staicu, L.C., Atasoy, M., Cetecioglu, Z., Kokko, M., Haznedaroglu, B.Z., Hansen, J., Istenič, D., Canga, E., Malamis, S., Camilleri-Fenech, M., Beesley, L., 2020. A review of nature-based solutions for resource recovery in cities. Blue-Green Syst. 2, 138–172. https://doi.org/10.2166/bgs.2020.930.

Kolbl, S., Panjan, J., Stres, B., 2016. Mixture of primary and secondary municipal wastewater sludge as a short-term substrate in 2 MW agricultural biogas plant: site-specific sustainability of enzymatic and ultrasound pretreatments. J. Chem. Technol. Biotechnol. 91, 2769–2778. https://doi.org/10.1002/jctb.4883.

Kumar, K., 2011. Influence of ultrasonic treatment in sewage sludge. J. Waste Water Treat. Anal. 02. https://doi.org/10.4172/2157-7587.1000115.

Lee, I., Han, J.I., 2013. The effects of waste-activated sludge pretreatment using hydrodynamic cavitation for methane production. Ultrason. Sonochem. 20, 1450–1455. https://doi.org/10.1016/j.ultsonch.2013.03.006.

Lee, G., Lee, I., Han, J.I., 2019. A combined method of hydrodynamic cavitation and alkaline treatment for waste-activated sludge solubilization; N/P recovery from anaerobic granular sludge. J. Environ. Chem. Eng. 7, 103329. https://doi.org/10.1016/j.jece.2019.103329.

Lorenz, C., Roscher, L., Meyer, M.S., Hildebrandt, L., Prume, J., Löder, M.G.J., Primpke, S., Gerdts, G., 2019. Spatial distribution of microplastics in sediments and surface waters of the southern North Sea. Environ. Pollut. 252, 1719–1729. https://doi.org/10.1016/j.envpol.2019.06.093.

Mitrano, D.M., Beltzung, A., Frehland, S., Schmiedgruber, M., Cingolani, A., Schmidt, F., 2019. Synthesis of metal-doped nanoplastics and their utility to investigate fate and behaviour in complex environmental systems. Nat. Nanotechnol. 14, 362–368. https://doi.org/10.1038/s41565-018-0360-3.

Mu, Y., Jia, F., Ai, Z., Zhang, L., 2017. Iron oxide shell mediated environmental remediation properties of nano zero-valent iron. Environ. Sci. Nano 4, 27–45. https://doi.org/10.1039/C6EN00398B.

Murphy, F., Ewins, C., Carbonnier, F., Quinn, B., 2016. Wastewater treatment works (WwTW) as a source of microplastics in the aquatic environment. Environ. Sci. Technol. 50, 5800–5808. https://doi.org/10.1021/acs.est.5b05416.

Official Gazette of the Republic of Slovenia: 62/2008. Government of the Republic of Slovenia, 2008. The use of sewage sludge in agriculture. https://www.uradni-list.si/1/objava.jsp?sop=2008-01-2630.

Parveen, T., Hussain, A., Rao, S., 2015. Growth and accumulation of heavy metals in turnip (Brassica rapa) irrigated with different concentrations of treated municipal waste water. Hydrol. Res. 46, 60–71. https://doi.org/10.2166/nh.2014.140.

Patil, P.B., Bhandari, V.M., Ranade, V.V., 2021. Improving efficiency for removal of ammoniacal nitrogen from wastewaters using hydrodynamic cavitation. Ultrason. Sonochem. 70, 105306. https://doi.org/10.1016/j.ultsonch.2020.105306.

Perwitasari, D.S., Muryanto, S., Jamari, J., Bayuseno, A.P., 2018. Kinetics and morphology analysis of struvite precipitated from aqueous solution under the influence of heavy metals: Cu2+, Pb2+, Zn2+. J. Environ. Chem. Eng. 6, 37–43. https://doi.org/10.1016/j.jece.2017.11.052.

Petkovšek, M., Mlakar, M., Levstek, M., Stražar, M., Širok, B., Dular, M., 2015. A novel rotation generator of hydrodynamic cavitation for waste-activated sludge disintegration. Ultrason. Sonochem. 26, 408–414. https://doi.org/10.1016/j.ultsonch.2015.01.006.

PROMEGA Application Note, https://worldwide.promega.com/resources/pubhub/enotes/how-do-i-determine-the-concentration-yield-and-purity-of-a-dna-sample/. (Accessed 22 October 2021).

R Core Team, 2020. R: A Language and Environment for Statistical Computing. R Foundation for Statistical Computing, Vienna, Austria.

Sabouhi, M., Ali-Taleshi, M.S., Bourliva, A., Nejadkoorki, F., Squizzato, S., 2020. Insights into the anthropogenic load and occupational health risk of heavy metals in floor dust of selected workplaces in an industrial city of Iran. Sci. Total Environ. 744, 140762. https://doi.org/10.1016/j.scitotenv.2020.140762.

Ščančar, J., Milačič, R., Stražar, M., Burica, O., Bukovec, P., 2001. Environmentally safe sewage sludge disposal: the impact of liming on the behaviour of Cd, Cr, Cu, Fe, Mn, Ni, Pb, and Zn. J. Environ. Monit. 3, 226–231. https://doi.org/10.1039/b008948f.

Sheng, G.P., Yu, H.Q., Li, X.Y., 2010. Extracellular polymeric substances (EPS) of microbial aggregates in biological wastewater treatment systems: a review. Biotechnol. Adv. 28, 882–894. https://doi.org/10.1016/j.biotechadv.2010.08.001.

Simon, M., van Alst, N., Vollertsen, J., 2018. Quantification of microplastic mass and removal rates at wastewater treatment plants applying Focal Plane Array (FPA)-based Fourier Transform Infrared (FT-IR) imaging. Water Res. 142, 1–9. https://doi.org/10.1016/j.watres.2018.05.019.

Tessier, A., Campbell, P.G.C., Bisson, M., 1979. Sequential extraction procedure for the speciation of particulate trace metals. Anal. Chem. 51, 844–851. https://doi.org/10.1021/ac50043a017.

Twardowski, M.S., Boss, E., Sullivan, J.M., Donaghay, P.L., 2004. Modeling the spectral shape of absorption by chromophoric dissolved organic matter. Mar. Chem. 89, 69–88. https://doi.org/10.1016/j.marchem.2004.02.008.

Vilarroig, J., Martínez, R., Zuriaga-Agustí, E., Torró, S., Galián, M., Chiva, S., 2020. Design and optimization of a semi-industrial cavitation device for a pretreatment of an anaerobic digestion treatment of excess sludge and pig slurry. Water Environ. Res. 92, 2060–2071. https://doi.org/10.1002/wer.1366.

Wang, B., Su, H., Zhang, B., 2021. Hydrodynamic cavitation as a promising route for wastewater treatment – a review. Chem. Eng. J. 412, 128685. https://doi.org/10.1016/j.cej.2021.128685.

Zevnik, J., Dular, M., 2020. Cavitation bubble interaction with a rigid spherical particle on a microscale. Ultrason. Sonochem. 69. https://doi.org/10.1016/j.ultsonch.2020.105252.

Zubrowska-Sudol, M., Dzido, A., Garlicka, A., Krawczyk, P., Stępien, M., Umiejewska, K., Walczak, J., Wołowicz, M., Sytek-Szmeichel, K., 2020. Innovative hydrodynamic disintegrator adjusted to agricultural substrates pre-treatment aimed at methane production intensification—Cfd modelling and batch tests. Energies 13. https://doi.org/10.3390/en13164256.

Zupanc, M., Kosjek, T., Petkovšek, M., Dular, M., Kompare, B., Širok, B., Stražar, M., Heath, E., 2014. Shear-induced hydrodynamic cavitation as a tool for pharmaceutical micropollutants removal from urban wastewater. Ultrason. Sonochem. 21. https://doi.org/10.1016/j.ultsonch.2013.10.025.

Zupanc, M., Pandur, Ž., Stepišnik Perdih, T., Stopar, D., Petkovšek, M., Dular, M., 2019. Effects of cavitation on different microorganisms: the current understanding of the mechanisms taking place behind the phenomenon. A review and proposals for further research. Ultrason. Sonochem. 57, 147–165. https://doi.org/10.1016/j.ultsonch.2019.05.009.

Zupanc, M., Petkovšek, M., Zevnik, J., Kozmus, G., Šmid, A., Dular, M., 2020. Anomalies detected during hydrodynamic cavitation when using salicylic acid dosimetry to measure radical production. Chem. Eng. J. 396. https://doi.org/10.1016/j.cej.2020.125389.

Øyvind, H., Harper, D.A.T., Ryan, P.D., 2001. PAST: paleontological statistics software package for education and data analysis.